Curved Boundary Layer Meshing for Adaptive Viscous Flow Simulations

O. Sahni*, X.J. Luo, K.E. Jansen, M.S. Shephard

Scientific Computation Research Center (SCOREC)

Rensselaer Polytechnic Institute, 110 8th street, Troy, NY 12180

Abstract

This paper presents an adaptive mesh control procedure suitable for use with higher-order finite element methods to solve viscous flow problems. The procedure presented is an appropriate combination of anisotropic and boundary layer mesh adaptation that accounts for the need to use curved mesh edges and faces to maintain the required geometric approximation and mesh gradation within the boundary layers. The paper first discusses the mesh adaptation tools needed to create effective adapted meshes for higher-order viscous flow simulations. Consideration is then given to an overview of the individual mesh adaptation components that are combined to create such meshes. Finally, example results are given to demonstrate the importance of the techniques in accurate computation of physical quantities of interest and to also show the effectiveness of the developed procedures in dealing with domains of arbitrary geometric complexity.

Key words:
mesh adaptivity, boundary layer mesh, mesh curving, higher-order analysis, viscous flow simulations

*Corresponding author

Email addresses: osahni@scorec.rpi.edu (O. Sahni), xluo@scorec.rpi.edu (X.J. Luo), kjansen@scorec.rpi.edu (K.E. Jansen), shephard@scorec.rpi.edu (M.S. Shephard)

1. Introduction

It is well known that the use of high-order discretization methods provide higher rates of solution convergence [1, 2] and when these methods are used in conjunction with properly constructed meshes improved levels of accuracy can be obtained for a given amount of computational effort. An often overlooked aspect of the use of high-order spatial discretizations is the requirement that the mesh representation to the geometry maintains the appropriate level of approximation to ensure the convergence and accuracy of the resulting solution. More specifically in the case of curved domains, this requires that properly curved mesh entities be used when higher than linear spatial discretizations are employed [3, 4]. Methods to execute mesh adaptation (refinement and coarsening) when curved elements are used has received some recent attention [5, 6].

In many classes of problems anisotropically adapted meshes are highly desirable since they can provide a given level of accuracy with one, or more, orders fewer elements when compared to isotropically adapted meshes [7, 8, 9, 10, 11, 12, 13, 14, 15, 16, 17]. In some cases it is also desirable to maintain some degree of structure to the mesh in critical regions so that specific levels of mesh gradation and/or control of element configuration can be maintained. Viscous flow simulations are a good example of such cases where it is found that carefully defined and controlled layered elements in meshes are most effective in resolving boundary layers [18, 19, 20, 21, 22, 23].

This paper presents a curved mesh adaptation procedure that is well suited for use in the adaptive solution of viscous flow problems on unstructured anisotropic meshes that include carefully controlled boundary layer elements which are also adapted. The next section (Section 2) introduces the key mesh adaptation components that must be properly integrated together to create the required meshes. Section 3 discusses each of the components focusing on specific developments required to ensure they can effectively work together. The results section first demonstrates the application of these methods on a simple geometry where it is possible to quantitatively show the importance of adapted meshes with curved boundary layer elements using quadratic spatial discretizations. The results section also shows a more practical example considering general three-dimensional domain as encountered in real cases to which current methods are applied to demonstrate their applicability.

2. Adaptive mesh control for viscous flow simulations

The goal of this work is to provide mesh adaptation procedures for higher-order viscous flow simulations on general three-dimensional curved geometries. The initial mesh in such simulations is automatically generated without detailed or expert level knowledge about specific problem case, and subsequently controlled through mesh adaptivity. Since the mesh element shape and configuration requirements in an adapted mesh are (at least) partly a function of the equation discretization methods used, there is a need to match to the capabilities of the mesh generation and adaptation methods that are going to be applied. The results presented in the paper employ a stabilized finite element formulation that can include linear, quadratic and cubic basis functions [24, 25]. The general requirements placed on the meshes under this formulation that is designed to yield a high level of accuracy for a given amount of computational effort include:

- Mesh anisotropy to bound the number of entities in the mesh, where the degree of anisotropy can range from none (isotropic) in some portions of the domain to aspect ratios, as measured by longest edge length divided by shortest height, of six or more orders of magnitude for thin boundary layers occurring near walls in high Reynolds number flows [26, 27]. Extreme levels of anisotropy is typically required in limited portions of the domain (such as in close proximity to viscous walls), while aspect ratios on the order of 100 or more can be common in larger portions of the domain (for example, in solution features of shear layers or shock waves).

- Mesh structure to control the configuration and variation of element sizes in multiple directions, particularly in critical boundary layer regions. In the case of the stabilized finite element methods used here, this consideration is not important for determination of the overall flow field, but is of importance in the calculation of the local parameters constructed in terms of derivatives of the field, e.g., wall shear stresses [16, 23].

- Mesh representation to ensure that the mesh entities (edges and faces) provide an appropriate geometric approximation to the underlying domain geometry. In the cases where higher than linear basis functions are used, the mesh edges and faces on curved domain boundaries need

to be curved using the same order to which the equations are discretized [3, 5].

The current state of the procedure presented requires that the initial mesh must be generated with a basic knowledge of those areas where extreme mesh anisotropy might be needed along with strong control of the element configuration and size variations or gradation. It also requires that the locations of such needs are constrained to be in close proximity of the domain boundaries. This is accomplished by the appropriate combination of a generalized boundary layer mesh generation procedure with an automatic unstructured anisotropic mesh generator [20, 28]. Given a CAD representation of the domain with basic boundary layer mesh specification the initial mesh is automatically generated. Since the mesh adaptation procedure is capable of anisotropically adapting in both the layered part and in the unstructured portion of the mesh, the only input required in initial mesh generation is the identification of portions where boundary layers may turn out to be important. With such information at hand, the structure associated with boundary layer elements can be maintained in desired areas when needed. Note that it is not a problem to request boundary layer elements where they are not needed as the adaptive procedures will determine that and in essence undo the layered part on the specific portions of the boundary that do not need them.

Given this starting point, the mesh adaptation procedure presented here consists of the following components:

- Error indication procedures capable of defining the desired anisotropic mesh size field. This step consists of estimating and/or obtaining an indication of the discretization error based on the quality of the computed solution (for example, see [1, 2, 29]).

- Mesh adaptation procedures that can modify the given mesh to match the requested anisotropic mesh size field. To support a full range of simulation types, the process of mesh adaptivity should also include incremental transfer of any needed solution fields on to modified mesh as it is adapted. Such a process of field transfers is generally more efficient and accurate than executing a global field transfer as an independent step after the mesh is fully adapted.

- In those cases where curved mesh edges and faces are required on curved boundaries, procedures that can ensure the curved elements to remain

valid during mesh adaptation. As it will become clear in the next section, the basic operations of mesh adaptation and mesh curving must specifically consider whether the elements being modified are inside or outside of the layered part of the mesh.

3. Mesh adaptation components

3.1. Unstructured anisotropic mesh adaptivity

Many physical problems of interest, especially in the field of fluid mechanics, involve anisotropic solution features, for example, boundary layers which form near the walls in viscous flows or shock waves in high speed flows. Such solution features are most effectively resolved using mesh elements which are properly oriented with a significant degree of anisotropy, i.e., different resolution in different local directions. Moreover, a prior knowledge of such features is often not available which creates a need for automatic and adaptive construction of anisotropic meshes. Mesh metric size field based anisotropic adaptive methods for real geometries have been developed with substantial progress [7, 8, 9, 10, 11, 12, 13, 14, 15, 16, 17]. The mesh metric field in the examples presented in this paper are based on examination of the Hessian of the solution field [13, 16].

The function of mesh adaptation is to convert a given mesh into the desired mesh consistent with the anisotropic mesh size field provided. To specify an anisotropic size distribution, a mesh metric field is defined with the help of second-order tensors, referred as *mesh metric tensor*. A mesh metric tensor prescribes the desired anisotropy at a point (e.g., see [30]). It is defined as a positive-definite symmetric matrix $\mathcal{M}$, whose associated quadratic form $\langle \boldsymbol{X}, \mathcal{M}\boldsymbol{X} \rangle = 1$, defines a mapping of an ellipsoid in the physical space into a unit sphere in the *transformed/metric* space, see Figure 1. In other words, any vector $\boldsymbol{X}$ at point P assumes a unit value where distances are measured in the metric space. The current adaptive procedure accepts a discretized anisotropic mesh size field as input and applies mesh modification operations on the mesh entities to force them to match the specified mesh sizes [13]. The stated goal of the adaptive meshing technique is to yield a mesh with regular elements in the metric space where each mesh edge $\boldsymbol{e}$ must satisfy: $\langle \boldsymbol{e}, \mathcal{M}\boldsymbol{e} \rangle = 1$ (in practice this criteria is relaxed to ensure that a mesh can be created, see [13]). The mesh modification logic includes the single step mesh modification operators of edge split, edge collapse, edge swap, face swap or region collapse and methods to ensure newly defined mesh vertices are

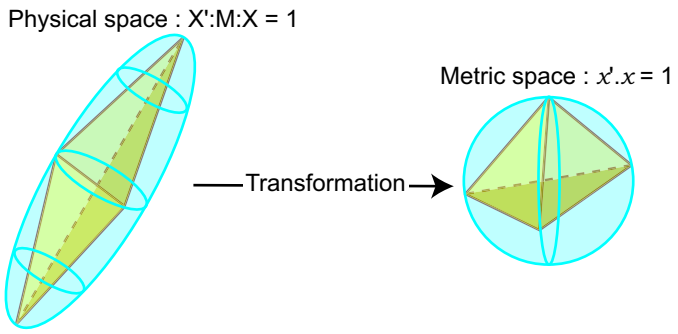

Figure 1: The transformation associated with a mesh metric tensor.

placed on the curved boundaries [12]. The procedure also includes selected compound operations such as edge split or swap followed by a collapse which have been found to be effective in modifying the mesh to satisfy the given anisotropic mesh size field.

The mesh modification procedure consists of interacting high level components: refinement, swapping, coarsening and projection of new boundary vertices. Simply put, refinement is applied when given mesh entities are larger than indicated by the local anisotropic mesh size field in specific directions. Refinement is always executed to ensure that the mesh is fine enough to satisfy the mesh size field. Swapping is useful to improve the alignment of mesh entities in the mesh to better match the local anisotropic mesh size field. Coarsening is applied when the current mesh entities are smaller than that required by the local mesh size field in specific directions. When mesh edges and faces on curved domain boundaries are refined, the new vertices are projected onto the curved boundaries. Since the projection process can create elements that do not match the mesh size field, or become invalid, the projection can force the local application of additional mesh modification operations [12]. The mesh modification procedure includes specific ordering and selection of operations to be able to most effectively satisfy the mesh metric field. The resulting adaptively defined anisotropic meshes have been used in a wide variety of physical problems [10, 11, 14, 15, 16, 17].

3.2. Boundary layer mesh adaptation

In the case of viscous flow simulations, better results for key quantities of interest in regions of boundary layers, like wall shear stress, can be obtained with the help of meshes with layered and graded elements near the viscous

walls. Favorable attributes of such meshes are high-aspect ratio, orthogonal, layered and graded elements near the walls for realistic geometries. Although it is not difficult to make an *a priori* specification of those portions of the domain boundary where such boundary layer meshes may be desired, knowledge of the required mesh resolution within those boundary layers for real cases is unknown *a priori*. To address this issue of boundary layers a mesh adaptation process that incorporates the capacity to preserve the layered structure when adapting the boundary layer mesh has been developed [16]. This procedure works in conjunction with the fully unstructured, anisotropic adaptive meshing technique discussed in the previous subsection.

The inherent structure in the boundary layer mesh allows it to be decomposed as a product of a layer surface (2D) mesh and a growth/thickness (1D) mesh that creates a stack of elements above each mesh face on the surface. Each stack is a set of elements in layers bounded by three segments of edges, referred to as growth curves moving into the domain form the vertices of a surface mesh face in a direction normal, or nearly normal, to the surface (see Figure 2). The stacks of elements are to remain as stacks during the boundary layer mesh adaptation process. Thus, the process of boundary layer mesh adaptation is decomposed into the two steps of surface adaptation and thickness adjustment that preserve the topological structure of the stacks of layered elements.

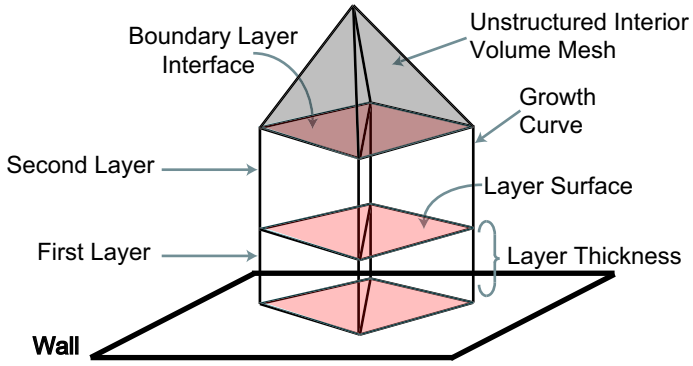

Figure 2: Decomposition of a boundary layer mesh.

This two step boundary layer adaptation procedure is governed by the mesh size field and applies similar concepts as the general unstructured anisotropic meshes. The local mesh modification operations of edge split,

edge collapse and edge swap are utilized to perform the surface mesh adaptation while node movement is applied to adjust the layer thicknesses. In case of surface mesh modification any operation is carried out such that it is propagated through the stack of boundary layer elements and affects all the layer surfaces along with the interface elements in the same way. For example, see Figure 3 where layer edge split operation is carried out on all the layers, including the interface elements. The figure depicts a stack before and after the application of layer edge split operation where three boundary

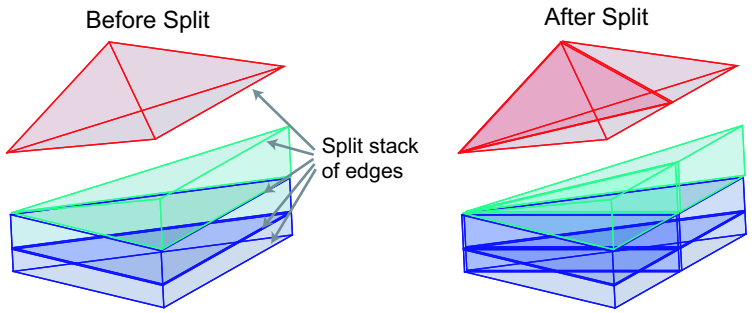

Figure 3: Stack of boundary layer and interface elements before (left) and after (right) the application of layer edge split operation (interface elements are offset from the boundary layer elements).

layer elements, i.e., two regular prisms and one transition pyramid, and one interface tetrahedron are subdivided. In the case of thickness adjustment the desired normal mesh resolution for each layer, and hence total thickness, is achieved by node movement (even for the top most node of the stack) while, currently, maintaining the number and topology of the layers as depicted in Figure 4.

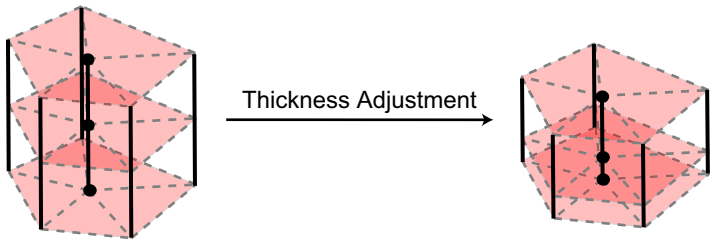

Figure 4: Schematic for thickness adjustment of a boundary layer mesh.

For geometries of interest that contain sharp and tight corners, care is required to produce elements of acceptable shape and to prevent element

overlap. Such cases are handled by terminating stacks of boundary layer elements through smoothly trimming them at the corners. Consideration is also given during the adaptation process to newly created vertices at curved boundaries such that they are projected on to the correct model surfaces. For more details on boundary layer mesh adaptivity see [23]. For curved domains, higher-order methods further require use of curved mesh entities with shapes that better represent the underlying geometry. The structure in boundary layer meshes, where there are highly anisotropic elements with short edges normal to the model surface, places additional control requirements on the curved mesh adaptation process as discussed in next section. Such an integration step of using mesh curving procedure on adapted boundary layer meshes has been lacking in previous studies.

3.3. Adaptation of curved meshes including layered elements

Higher-order discretization methods require mesh representation in terms of curved element shapes on curved domain boundaries to maintain the appropriate level of convergence and accuracy of the resulting solution [3]. The most effective approach to construct such (curved) meshes is to start from linear straight-sided meshes that are altered by assigning higher-order shape to the mesh edges and faces at the curved boundaries. Since the simple assignment of higher-order shape to mesh entities often leads to invalid (see Figure 3.3), or undesirably shaped (curved) elements, a mesh modification based mesh curving procedure is required to ensure that valid and acceptable meshes with curved mesh entities are produced [5].

To maintain the validity of curved mesh entities the current algorithm ensures that each curved element has positive determinant of Jacobian in its closure. Since higher-order methods such as finite elements use basis functions and integration schemes of their choice, an effective algorithm to verify the validity of curved meshes that is independent of the basis functions or integration rules is desirable. A global validity check algorithm of Bézier higher-order elements is employed that takes advantage of the convex hull property to ensure positive determinant of Jacobian [5].

For example, given a *qth* order Bézier mesh tetrahedral region as,

$$\boldsymbol{x}(\boldsymbol{\xi}) = \sum_{|\boldsymbol{i}|=q} B_{|\boldsymbol{i}|}(\boldsymbol{\xi}) b_{|\boldsymbol{i}|} \boldsymbol{\xi}^{|\boldsymbol{i}|} \tag{1}$$

where, $\boldsymbol{\xi} = (\xi_1, \xi_2, \xi_3, \xi_4)$ are the parametric coordinates with $\xi_1+\xi_2+\xi_3+\xi_4 = 1$, $|\boldsymbol{i}| = i + j + k + l$, $B_{|\boldsymbol{i}|} = \frac{q!}{i!j!k!l!}$ and $\boldsymbol{\xi}^{|\boldsymbol{i}|} = \xi_1^i \xi_2^j \xi_3^k \xi_4^l$. $b_{|\boldsymbol{i}|}$ are the control

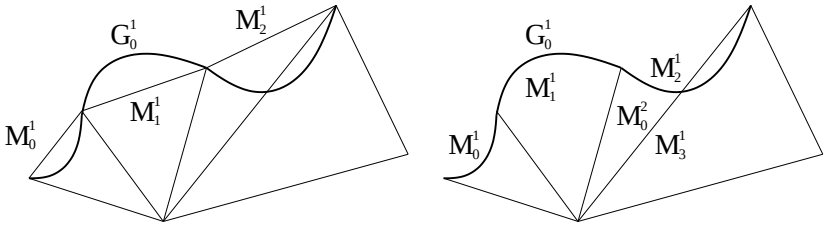

(a) Initial straight-sided mesh

(b) Curve M_0^1, M_1^1 and M_2^1

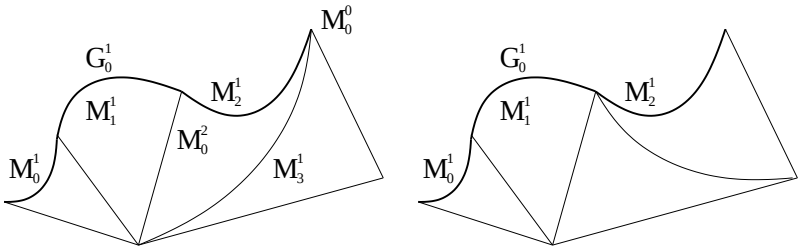

(c) Curve M_3^1 to correct invalid element M_0^2

(d) Swap and curve M_3^1 to correct invalid element M_0^2

Figure 5: Curve the mesh entities that lie on curved domain boundaries.

points used to define the shapes of the Bèzier. The Jacobian matrix of the geometric mapping with respect to the independent set of parametric coordinates (ξ_1, ξ_2, ξ_3) is,

$$J = \left[\frac{\partial \mathbf{x}}{\partial \xi}\right] = \begin{bmatrix} \frac{\partial x_1}{\partial \xi_1} & \frac{\partial x_1}{\partial \xi_2} & \frac{\partial x_1}{\partial \xi_3} \\ \frac{\partial x_2}{\partial \xi_1} & \frac{\partial x_2}{\partial \xi_2} & \frac{\partial x_2}{\partial \xi_3} \\ \frac{\partial x_3}{\partial \xi_1} & \frac{\partial x_3}{\partial \xi_2} & \frac{\partial x_3}{\partial \xi_3} \end{bmatrix} \tag{2}$$

where $\mathbf{x} = (x_1, x_2, x_3)$ Therefore, the determinant of the Jacobian J is,

$$det(J) = (\frac{\partial \boldsymbol{x}}{\partial \xi_1} \times \frac{\partial \boldsymbol{x}}{\partial \xi_2}) \cdot (\frac{\partial \boldsymbol{x}}{\partial \xi_3}) \tag{3}$$

where $\frac{\partial \boldsymbol{x}}{\partial \xi_i}$ are the three partial derivatives of $\boldsymbol{x}^q$ which are $(q-1)th$ order Bézier functions. Therefore, the resulting determinant of Jacobian is a Bézier polynomial function with order $3(q-1)$,

$$det(J) = \sum_{|\boldsymbol{i}|=r} C_{|\boldsymbol{i}|} c_{|\boldsymbol{i}|} \boldsymbol{\xi}^{|\boldsymbol{i}|} \tag{4}$$

where $r = 3(q-1)$. $C_{|\boldsymbol{i}|}$ and $c_{|\boldsymbol{i}|}$ can be expressed using the coefficients $B_{|\boldsymbol{i}|}$ and $b_{|\boldsymbol{i}|}$ present in Eq. 1. The convex hull property of Bézier polynomial indicates that the polynomial is bounded by its minimal and maximal control points [31]. So,

$$min(c_{|\boldsymbol{i}|}) \leq det(J) \leq max(c_{|\boldsymbol{i}|}) \tag{5}$$

Therefore, a curved tetrahedral region is valid in its closure as long as its $min(c_{|\boldsymbol{i}|}) > 0$.

The basic steps involved in the process of correcting an invalid element are:

- Determination of key mesh entities in the closure of an invalid element needs to be considered in order to correct it through suitable local mesh modifications. The computation of the determinant of Jacobian to detect invalid elements can provide useful information to determine key mesh entities and appropriate operations to correct the invalidity. The invalid elements are defined as those curved elements that have at least one zero or negative coefficient, $c_{|\boldsymbol{i}|} \leq 0$ as shown in Eq. 4. The key mesh entities are defined as ones (with control points) that lead to negative determinant of Jacobian within the element.

- Application of a set of local mesh modifications to eliminate any given invalid curved element. The type of operations applied and the order of application is a function of the key mesh entities determined in the first step. The set of mesh modification operators employed in this step include edge split, edge swap, edge collapse, region collapse, double split with a collapse, and edge re-shape. All operations include specific consideration of the existence of curved mesh entities making them more complex than any corresponding straight edged mesh modification operation. The validity check algorithm discussed above is used to determine whether a curved local mesh modification operation can be applied. Those operations are essential to ensure the reliability of the mesh curving procedure to create valid curved elements.

In the case of meshes with highly anisotropic boundary layer elements, the application of the general unstructured mesh curving procedures not only results in invalid mesh but also destroys the boundary layer stack structure (as shown in Figures 6(b) and 6(e)). Thus, there are additional control requirements to generate valid curved elements and at the same time preserve the structure in the boundary layer mesh. Mesh curving procedure for boundary layer meshes is executed in the following three steps:

- Curving of straight-sided boundary layer elements including mesh entities on the domain boundaries and those in the stack of layers (see Figures 6(c) and 6(f)).

- Curving of the remaining (non-boundary layer) mesh edges/faces that lie on curved domain boundaries.

- Application of a fixed set of local mesh modification operators (as discussed above) to incrementally correct the invalid elements created in the previous two steps.

The first two steps require defining higher-order shapes for mesh entities throughout the boundary layer stack. Bernstein polynomials are used to effectively construct Bézier hierarchic higher order shapes for topological mesh entities on the model boundaries and those within the boundary layers [5]. The procedure starts from curving the mesh entities on the domain boundaries and those within the above stack of layer elements. The control points of the edges in the stack of layer elements are moved based on control points

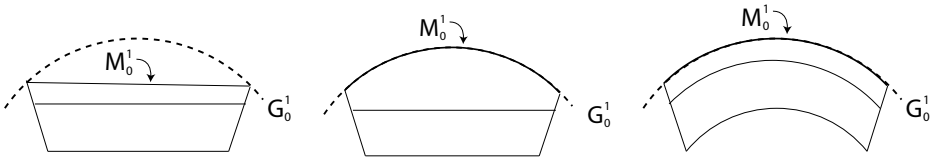

(a) Case a: Straight-sided BL mesh

(b) Case a: Curving only M_0^1 to G_0^1

(c) Case a: Curving stack of boundary layer elements

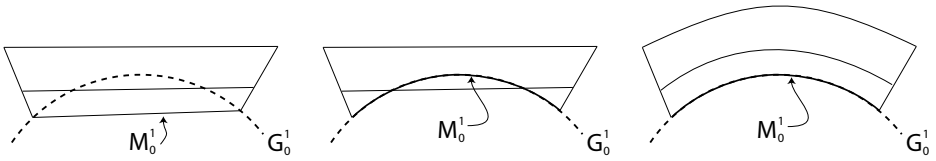

(d) Case b: Straight-sided BL mesh

(e) Case b: Curving only M_0^1 to G_0^1

(f) Case b: Curving stack of boundary layer elements

Figure 6: Smoothly curving a stack of boundary layer elements.

of the base edge at the boundary where consideration is given to the change in length of the edges being curved to alter the degree of curving of interior entities. Figures 6(c) and 6(f) show stack of smoothly curved boundary layer elements created by using this method.

Figures 7 and 8 demonstrate the application of the boundary layer curving procedure. Figure 7 shows a straight-sided boundary layer mesh which has been curved with/without considering the stack of layer elements. Figure 7(c) also demonstrates that only curving the mesh entities at domain boundaries leads to invalid elements whereas Figure 7(d) shows that properly curving the stack of layer elements avoids this problem. Figure 8 further demonstrates the effectiveness of curving a stack of layer elements (including in the clip view).

4. Flow applications

This section first demonstrates the application of meshing techniques described in the previous section on an example with flow in a simple geometry of straight pipe. This simple case is selected because it allows to quantitatively access the importance of adapted meshes with curved boundary layer elements using quadratic spatial discretizations. A more practical example of cardiovascular flow in a subject-specific healthy human abdominal aorta is then considered where current methods are applied to demonstrate their applicability to general three-dimensional domains encountered in real problems.

4.1. Flow in a straight pipe

A steady fully-developed incompressible laminar flow within a straight pipe is considered where exact solution of paraboloid flow profile is well known (commonly referred to as Hagen-Poiseuille flow). The length of the pipe considered is $L = 10cm$ and radius is $r = 1cm$. A paraboloid profile with a unit peak is prescribed at the inlet while no-slip conditions are assumed on the outer cylindrical wall and the outflow has a zero natural pressure condition. The viscosity and density are assumed to be $\mu = 0.01 dynes\ s/cm^2$ and $\rho = 1g/cm^3$, respectively. The velocity field only has a single non-zero component (the axial component) and this component is constant in axial direction due to fully developed nature of the flow, thus varying only radially. Therefore, the wall shear stress magnitude assumes a constant value

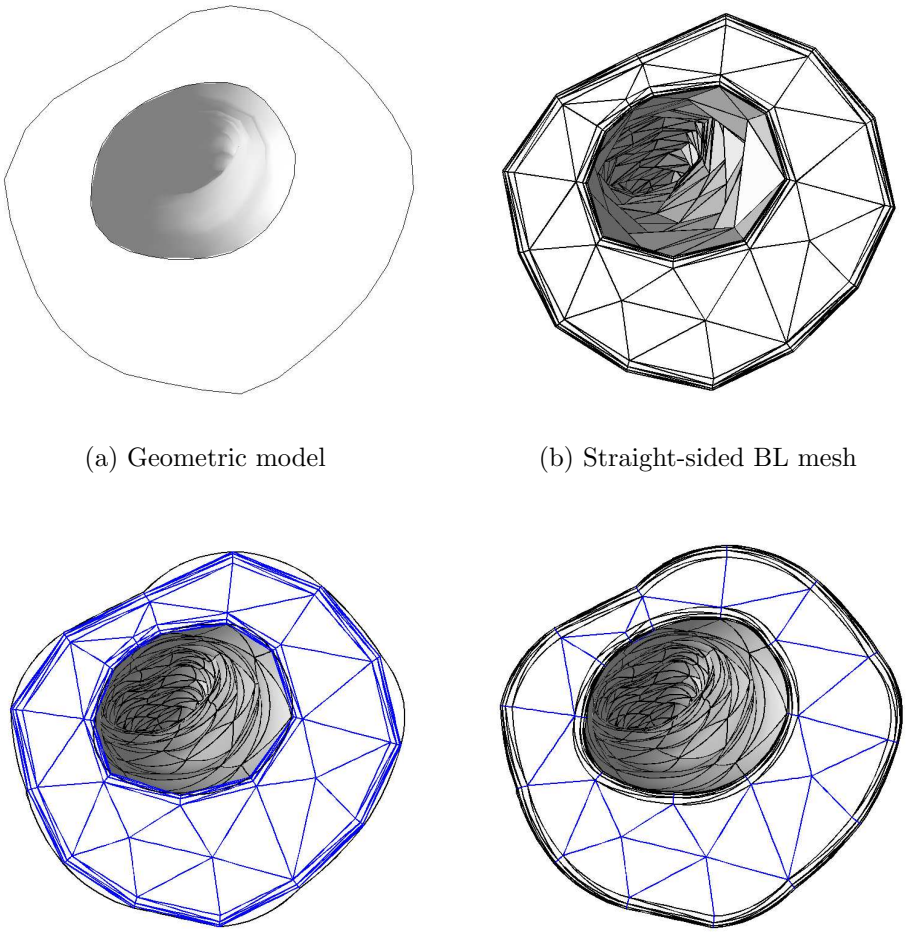

(a) Geometric model

(b) Straight-sided BL mesh

(c) Curved mesh (without curving of stacks)

(d) Curved BL mesh (with curving of stacks)

Figure 7: Spine fluid flow model: (a) geometric model, (b) straight-sided mesh, (c) curved mesh and (d) curved boundary layer (BL) mesh.

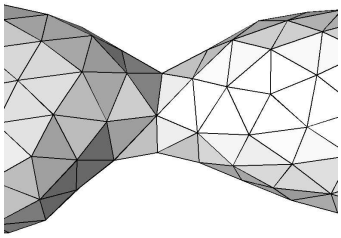

(a) Zoom of straight-sided BL mesh near stenosis

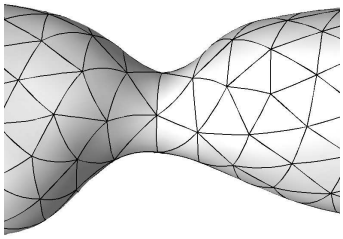

(b) Zoom of curved BL mesh near stenosis

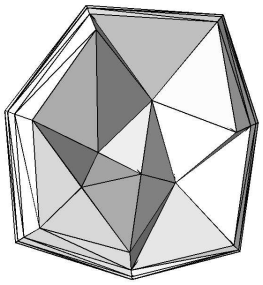

(c) Clip view of straight-sided BL mesh at stenosis

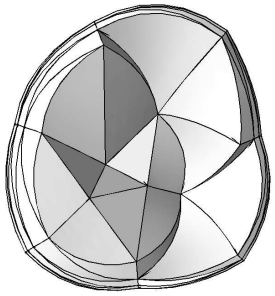

(d) Clip view of curved BL mesh at stenosis

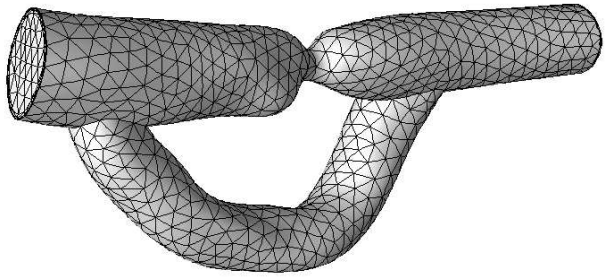

(e) Surface of curved BL mesh

Figure 8: Straight-sided and curved boundary layer meshes for porcine aorta with a stenosis bypassed by a graft.

of $t_w = 2\mu = 0.02 dynes/cm^2$ over the entire cylindrical wall creating a axial force of $f = A\, t_w = 2\pi r L\, 2\mu = 1.256637\ dynes$ (due to viscous shear stress).

Flow computations are performed using a stabilized, semi-discrete finite element method for the incompressible Navier-Stokes equation governing viscous flows. In particular, we employ the streamline upwind/Petrov-Galerkin (SUPG) stabilization method introduced in [32] to discretize the governing equations. The stabilized finite element formulation currently utilized has been shown to be robust, accurate and stable on a variety of flow problems (see for example [24, 33]). Same order basis functions, both for the pressure and the velocity fields, are used in these computations (note that equal-order interpolation for both fields is possible as SUPG stabilized formulation is employed).

Three different solution strategies are exercised based on combinations of order employed for element shape (referred as q, where $q = 1$ implies straight-sided elements whereas $q = 2$ implies quadratic curved elements) and basis functions (referred as p, where $p = 1$ is linear and $p = 2$ is quadratic). The three cases are $q1 - p1$, $q1 - p2$ and $q2 - p2$ where the first two combinations use straight-sided elements and the last one with $q = 2$ uses quadratic curved elements. Further, in order to perform quantitative comparison four adapted boundary layer meshes with different resolutions are used in each solution strategy. These meshes are constructed through anisotropic adaptation such that mesh resolution (or element size) in the axial direction is constant and much higher than the uniform resolution in the cross-section (for details on mesh adaptivity see [16]). The four meshes considered are successive sub-division of edges in the cross-section with the coarsest mesh containing roughly 10 mesh edges across a diameter with $h = 0.2$ as shown in Figure 9 and thus, subsequent meshes have size of $h = 0.1$ (20 edges across diameter), $h = 0.05$ (40 edges across diameter) and $h = 0.025$ (80 edges across diameter). Since the flow is fully developed in nature, the element size along the axis is fixed at $h_{axial} = 2.5$ (i.e., 4 edges along the axis).

Table 1 provides the computed values of the axial force over four adapted boundary layer meshes for each solution strategy. The relative error in the computed axial force ($e_i = |f_i - f_{exact}|/f_{exact}$) is provided in Table 2 and also shown in Figure 10. Note that the axial force is due to the wall shear stresses that in turn involves derivatives of velocity field and thus, its optimal rate of convergence is proportional to the discretization order used in numerical methods such as finite elements. Figure 10 clearly shows the advantage of using curved elements in adapted boundary layer meshes as it allows to

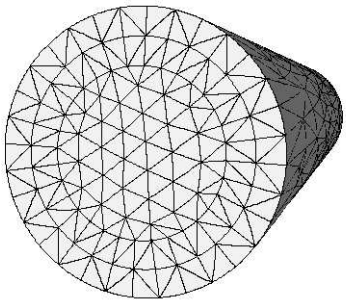

Figure 9: Coarsest adapted boundary layer mesh ($h = 0.2$) used in straight pipe example.

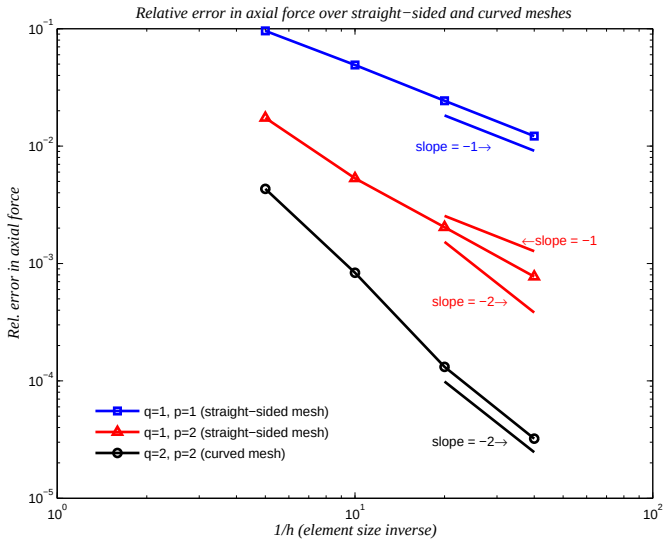

Figure 10: Relative error in axial force computed over straight-sided and curved meshes (for reference ideal slope lines for first- and second-order discretizations are provided).

Table 1: Axial force computed over straight-sided and curved meshes.

Mesh Solution strategy	$q1-p1$	$q1-p2$	$q2-p2$
$Mesh_{A0}$ $(h=0.200)$	1.136180	1.278480	1.262070
$Mesh_{A1}$ $(h=0.100)$	1.195020	1.263310	1.255590
$Mesh_{A2}$ $(h=0.050)$	1.226073	1.259196	1.256472
$Mesh_{A3}$ $(h=0.025)$	1.241358	1.257607	1.256597

Table 2: Relative error in axial force computed over straight-sided and curved meshes.

Mesh Solution strategy	$q1-p1$	$q1-p2$	$q2-p2$
$Mesh_{A0}$ $(h=0.200)$	9.586e-2	1.738e-2	4.323e-3
$Mesh_{A1}$ $(h=0.100)$	4.903e-2	5.310e-3	8.332e-4
$Mesh_{A2}$ $(h=0.050)$	2.432e-2	2.036e-3	1.315e-4
$Mesh_{A3}$ $(h=0.025)$	1.216e-2	7.716e-4	3.218e-5

reach the optimal rate of convergence whereas the rate of convergence for a straight-sided mesh with quadratic basis functions is sub-optimal (for reference ideal slope lines for first- and second-order discretizations are provided in Figure 10).

4.2. Blood flow in a healthy human abdominal aorta

This example is considered to demonstrate the applicability of current adaptive meshing techniques for high-order simulations of viscous flows in practical problems of interest. Cardiovascular flow in a subject-specific case of healthy human abdominal aorta is considered. The anatomic model of the subject-specific abdominal aorta with various branches is shown in Figure 11. The main trunk is approximately $30cm$ long with a diameter of $2.5cm$ at the inlet (which is non-circular). The length of the branches varies from $1.8cm$ to $5cm$ whereas their diameter lies roughly between $0.3-0.8cm$. The waveform of the volumetric flow rate at the inlet is shown in the inset within Figure 11, which is derived from the imaging data [34], with a time period $t_p = 1.05s$; and a peak and trough of around $150cc/s$ and $10cc/s$, respectively. The inset also shows two instants: peak systole, which is the heart contraction phase, and early diastole, which is the dilatation phase. No-slip conditions are assumed on the vessel walls and impedance boundary conditions are prescribed at the outlets [35] (where an electric circuit analog of an impedance, i.e., a

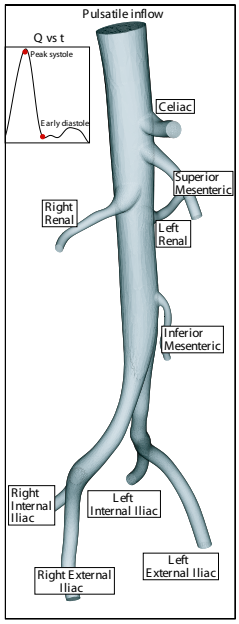

Figure 11: Anatomic model of a healthy human abdominal aorta with various branches. The inset shows the volumetric flow rate at the inlet (the two dots in the inset correspond to instants of peak systole and early diastole).

measure of opposition to motion by a system, is applied to relate downstream pressure with the flow rate). The viscosity and density are assumed to be $\mu = 0.04 dynes\ s/cm^2$ and $\rho = 1.06 g/cm^3$, respectively.

Similar to the previous example, we employ the streamline upwind/Petrov-Galerkin (SUPG) stabilization method introduced in [32] to discretize the governing equations. As the blood flow is unsteady in nature, a second-order generalized-α time integrator [36] is used that turns the system of non-linear ordinary differential equations obtained via spatial discretization in a non-linear system of algebraic equations. This system is in turn linearized with Newton's method to obtain a linear algebraic system of equations that is solved using a custom linear algebra solver [37]. In such cases, typically four to five cardiac cycles are simulated to obtain a periodic flow in time. Current computations used 105 time steps in a cardiac cycle with equal time step size of $0.01s$.

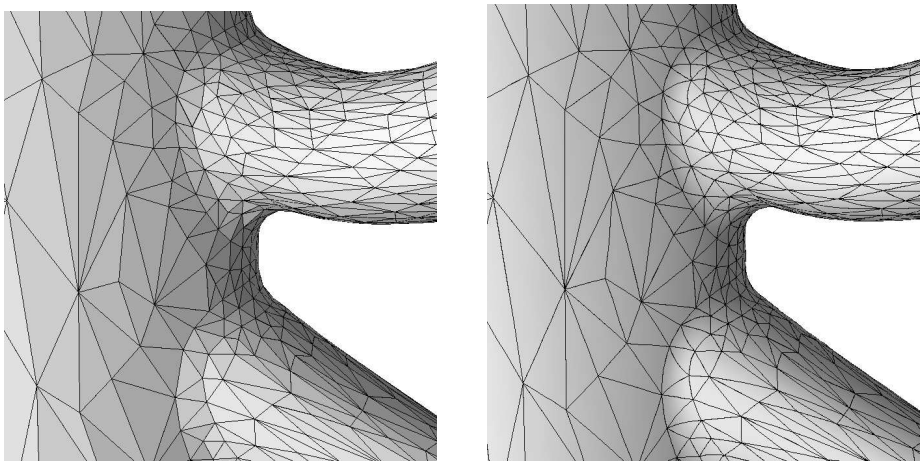

(a) Zoom of straight-sided BL adapted mesh near celiac

(b) Zoom of curved BL adapted mesh near celiac

Figure 12: Surface of straight-sided and curved adapted boundary layer (BL) meshes near celiac branch in case of a healthy human abdominal aorta.

Adapted boundary layer meshes obtained after two iterations of flow computations and mesh adaptation are shown in Figures 12, 13 and 14. In all figures, curved adapted mesh with quadratic elements is shown along with

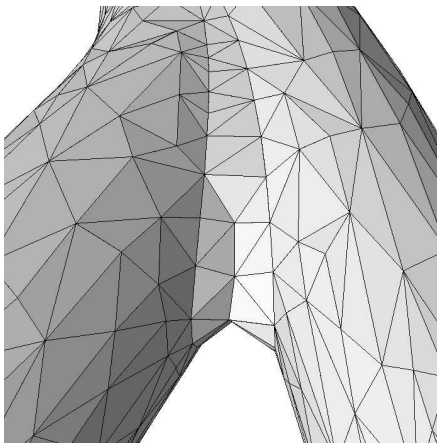

(a) Zoom of straight-sided BL adapted mesh near iliac

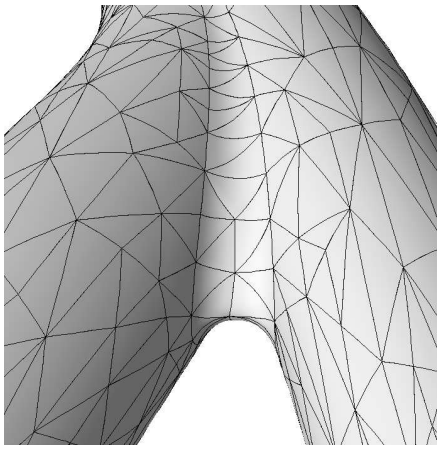

(b) Zoom of curved BL adapted mesh near iliacs

Figure 13: Surface of straight-sided and curved adapted boundary layer meshes near iliac branches in case of a healthy human abdominal aorta.

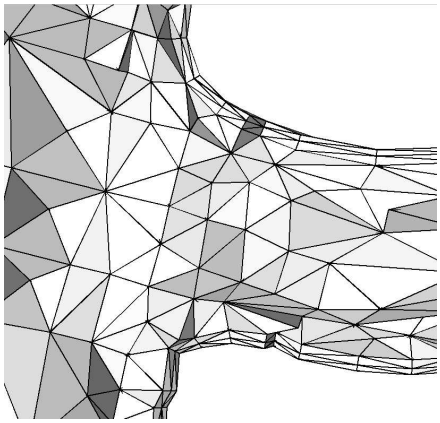

(a) Clip view of straight-sided BL adapted mesh at celiac

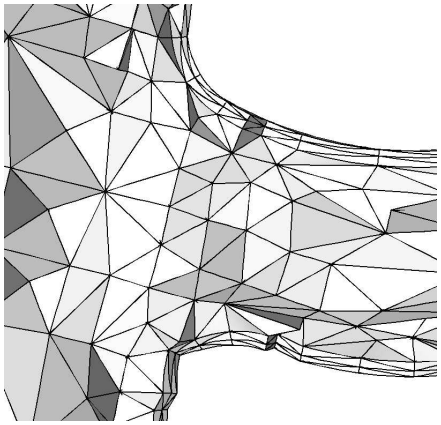

(b) Clip view of curved BL adapted mesh at celiac

Figure 14: Clip view of straight-sided and curved adapted boundary layer meshes in case of a healthy human abdominal aorta.

straighted-sided one for comparison. Figures 12 and 13 show the surface of the adapted mesh near arterial branches of celiac and iliac (as labeled in Figure 11) whereas Figure 14 provides a clip view to show the interior mesh within the domain. The mesh representation with improved level of geometric approximation can be clearly seen in case of curved adapted boundary layer mesh using quadratic elements. This case demonstrates the applicability of current meshing techniques to general three-dimensional domains encountered in real problems.

5. Closing remarks

This paper presented a meshing technique that applies mesh curving procedure on adapted boundary layer meshes to allow for higher-order analysis of viscous flows. The procedures developed account for the layered structure of anisotropic elements in the boundary layer meshes to be able to construct elements with proper configuration and gradation. The benefits of using curved boundary layer adapted meshes were quantitatively demonstrated on derived near-wall quantities of interest, such as shear force or wall shear stress, for an example considering flow in a simple geometry of straight pipe. The current techniques were then applied to a more practical example of cardiovascular flow in a subject-specific healthy human abdominal aorta to demonstrate the effectiveness of techniques to general three-dimensional domains for real problems.

Acknowledgments

This work is supported in part by U.S. Department of Energy under DOE grant number DE-FC02-06ER25769 and by NSF under grants OCI-0749152 and ACI-0205741. Computing support at the Rensselaer Computational Center for Nanotechnology Innovations was funded in part by the State of New York. The results presented in this article made use of the linear algebra library provided by ACUSIM Software Inc. We would also like to acknowledge that we made use of software tools provided by Simmetrix Inc. for visualization of curved meshes.

References

[1] B. Szabo, I. Babuška, Finite Element Analysis, Wiley, New York, 1991.

[2] M. Ainsworth, J. Oden, A Posteriori Error Estimation in Finite Element Analysis, Wiley, 2000.

[3] S. Dey, M. Shephard, J. Flaherty, Geometry representation issues associated with p-version finite element computations, Comp. Meth. Appl. Mech. Engng. 150 (1-4) (1997) 39–55.

[4] X.-J. Luo, M. Shephard, J.-F. Remacle, R. O'Bara, M. Beall, B. Szabo, R. Actis, p-version mesh generation issues, in: Proc. 11th International Meshing Roundtable, Ithaca, NY, USA, 2002.

[5] X.-J. Luo, M. Shephard, R. O'Bara, R. Nastasia, M. Beall, Automatic p-version mesh generation for curved domains, Engineering with Computers 20 (3) (2004) 273–285.

[6] M. Shephard, J. Flaherty, K. Jansen, X. Li, X.-J. Luo, N. Chevaugeon, J.-F. Remacle, M. Beall, R. O'Bara, Adaptive mesh generation for curved domains, J. for Applied Numerical Mathematics 53 (2-3) (2005) 251–271.

[7] J. Peraire, M. Vahdati, K. Morgan, O. C. Zienkiewicz, Adaptive remeshing for compressible flow computations, Journal of Computational Physics 72 (1987) 449–466.

[8] G. C. Buscaglia, E. A. Dari, Anisotropic mesh optimization and its application in adaptivity, Int. J. Numer. Meth. Engng. 40 (1997) 4119–4136.

[9] M. J. Castro-Diáz, F. Hecht, B. Mohammadi, O. Pironneau, Anisotropic unstructured mesh adaption for flow simulations, International Journal of Numerical Methods in Fluids 25 (1997) 475–491.

[10] C. C. Pain, A. P. Umpleby, C. R. E. de Oliveira, A. J. H. Goddard, Tetrahedral mesh optimisation and adaptivity for steady-state and transient finite element calculations, Comp. Meth. Appl. Mech. Engng. 190 (2001) 3771–3796.

[11] J. F. Remacle, X. Li, M. S. Shephard, J. E. Flaherty, Anisotropic adaptive simulation of transient flows using Discontinuous Galerkin methods, Int. J. Numer. Meth. Engng. 62 (2005) 899–923.

[12] X. Li, M. S. Shephard, M. W. Beall, Accounting for curved domains in mesh adaptation, Int. J. Numer. Meth. Engng. 58 (2003) 247–276.

[13] X. Li, M. S. Shephard, M. W. Beall, 3D anisotropic mesh adaptation by mesh modifications, Comp. Meth. Appl. Mech. Engng. 194 (2005) 4915–4950.

[14] P. J. Frey, F. Alauzet, Anisotropic mesh adaptation for CFD computations, Comp. Meth. Appl. Mech. Engng. 194 (2005) 5068–5082.

[15] J. Mueller, O. Sahni, X. Li, K. Jansen, M. Shephard, C. Taylor, Anisotropic adaptive finite element method for modeling blood flow, Comp. Meth. in Biomech. and Biomed. Engng. 8 (5) (2005) 295–305.

[16] O. Sahni, J. Mueller, K. Jansen, M. Shephard, C. Taylor, Efficient anisotropic adaptive discretization of cardiovascular system, Comp. Meth. Appl. Mech. Engng. 195 (41-43) (2006) 5634–5655.

[17] C. Dobrzynski, P. Frey, Anisotropic delaunay mesh adaptation for unsteady simulations, in: Proc. 11th International Meshing Roundtable, Pittsburgh, PA, USA, 2008.

[18] S. Pirzadeh, Unstructured viscous grid generation by the advancing-layers method, AIAA Journal 32 (1994) 1735–1737.

[19] B. M. Connell SD, Semi-structured mesh generation for three-dimensional Navier-Stokes calculations, AIAA Journal 33 (1995) 1017–1024.

[20] R. V. Garimella, M. S. Shephard, Boundary layer mesh generation for viscous flow simulations, Int. J. Numer. Meth. Engng. 49 (2000) 193–218.

[21] Y. Ito, K. Nakahashi, Unstructured mesh generation for viscous flow computations, in: Proc. 11th Internatinal Meshing Roundtable, Ithaca, NY, USA, 2002.

[22] Y. Kallinderis, C. Kavouklis, A dynamic adaptation scheme for general 3-D hybrid meshes, Comp. Meth. Appl. Mech. Engng. 194 (2005) 5019–5050.

[23] O. Sahni, K. Jansen, M. Shephard, C. Taylor, M. Beall, Adaptive boundary layer meshing for viscous flow simulations, Engng. with Comp. 24 (3) (2008) 267–285.

[24] C. H. Whiting, K. E. Jansen, A stabilized finite element method for the incompressible Navier-Stokes equations using a hierarchical basis, International Journal of Numerical Methods in Fluids 35 (2001) 93–116.

[25] C. H. Whiting, K. E. Jansen, S. Dey, Hierarchical basis in stabilized finite element methods for compressible flows, Comp. Meth. Appl. Mech. Engng. 192 (2003) 5167–5185.

[26] N. T. Frink, Assessment of an unstructured-grid method for predicting 3-D turbulent viscous flows, in: AIAA Paper 96-0292, 1996.

[27] K. E. Jansen, M. S. Shephard, M. W. Beall, On anisotropic mesh generation and quality control in complex flow problems, in: Proc. 10th Internatinal Meshing Roundtable, Newport Beach, CA, USA, 2001.

[28] Simmetrix, http://www.simmetrix.com, Simmetrix Inc., 10 Halfmoon Executive Park Drive, Clifton Park, NY 12065, USA.

[29] R. Verfürth, A Review of Posteriori Error Estimation and Adaptive Mesh-Refinement Techniques, Teubner-Wiley, Stuttgart, 1996.

[30] H. Borouchaki, P.-L. George, B. Mohammadi, Delaunay mesh generation governed by metric specifications. Part II. Applications, Finite Elements in Analysis and Design 25 (1997) 85–109.

[31] G. Farin, Curves and Surfaces for Computer Aided Geometric Design, Academic Press, 1992.

[32] A. N. Brooks, T. J. R. Hughes, Streamline upwind / Petrov-Galerkin formulations for convection dominated flows with particular emphasis on the incompressible Navier-Stokes equations, Comp. Meth. Appl. Mech. Engng. 32 (1982) 199–259.

[33] C. A. Taylor, T. J. R. Hughes, C. K. Zarins, Finite element modeling of blood flow in arteries, Comp. Meth. Appl. Mech. Engng. 158 (1998) 155–196.

[34] B. T. Tang, C. P. Cheng, M. T. Draney, N. M. Wilson, P. S. Tsao, R. J. Herfkens, C. A. Taylor, Abdominal aortic hemodynamics in young healthy adults at rest and during lower limb exercise: quantification using image-based computer modeling, Am. J. Physiol. Heart Circ. Physiol. 291 (2) (2006) H668–H676.

[35] I. Vignon-Clementel, C. Figueroa, K. Jansen, C. Taylor, Outflow boundary conditions for three-dimensional finite element modeling of blood flow and pressure in arteries, Comp. Meth. Appl. Mech. Engng. 195 (2006) 3776–3796.

[36] K. E. Jansen, C. H. Whiting, G. M. Hulbert, A generalized-α method for integrating the filtered Navier-Stokes equations with a stabilized finite element method, Comp. Meth. Appl. Mech. Engng. 190 (1999) 305–319.

[37] ACUSIM, http://www.acusim.com, 2685 Marine Way, Suite 1421, Mountain View, CA 94043, USA.